A role of gut–microbiota–brain axis via subdiaphragmatic vagus nerve in depression-like phenotypes in *Chrna7* knock-out mice

（α7 ニコチン受容体遺伝子欠損マウスのうつ様行動における横隔膜迷走神経を介する腸-脳相関の役割）

千葉大学大学院医学薬学府

先端医学薬学専攻

（主任：橋本 謙二 教授）

楊 勇

Abstract

The α7 subtype of the nicotinic acetylcholine receptor (α7 nAChR: coded by *Chrna7*) is known to regulate the cholinergic ascending anti-inflammatory pathway. We previously reported that *Chrna7* knock-out (KO) mice show depression-like behaviors through abnormal composition of gut microbiota and systemic inflammation. Given the role of subdiaphragmatic vagus nerve in gut–microbiota–brain axis, we investigated whether subdiaphragmatic vagotomy (SDV) could affect depression-like behaviors, abnormal composition of gut microbiota, and microbes-derived metabolites in *Chrna7* KO mice. SDV blocked depression-like behaviors and reduced expression of synaptic proteins in the medial prefrontal cortex (mPFC) of *Chrna7* KO mice. LEfSe (linear discriminant analysis effect size) analysis revealed that the species *Lactobacillus sp. BL302*, the species *Lactobacillus hominis*, and the species *Lactobacillus reuteri*, were identified as potential microbial markers in the KO + SDV group. There were several genus and species altered among the three groups [wild-type (WT) + sham group, KO + sham group, KO + SDV group]. Furthermore, there were several plasma metabolites altered among the three groups. Moreover, there were correlations between relative abundance of several microbiome and behavioral data (or synaptic proteins). Network analysis showed correlations between relative abundance of several microbiome and plasma metabolites (or behavioral data). These data suggest that *Chrna7* KO mice produce depression-like behaviors and reduced expression of synaptic proteins in the mPFC through gut–microbiota–brain axis via subdiaphragmatic vagus nerve.

Keywords: α7 nAchR; brain-gut axis; gut microbiota; metabolites; vagus nerve.

Introduction

Depression is the most prevalent mental disorder with an estimated 5.0 % of adults and 5.7 % of elderly adults (> 60 years old) worldwide. Furthermore, depression is a leading cause of disability worldwide, and it is a major contributor to the overall global burden of disease (WHO 2021). Although the precise neurobiology underlying depression remains unclear, inflammation is known to play an important role in depression (Brydges et al., 2022; Haroon et al., 2012; Hashimoto, 2009; Hashimoto, 2015; Liu et al., 2020; Lucido et al., 2021; Mac Giollabhui et al., 2021; Miller and Raison, 2016; Shan and Hashimoto, 2022; Toenders et al., 2022; Zhang et al., 2016a).

Nicotinic acetylcholine receptor (nAChR) is a kind of ionotropic ligand-gated ion channels widely distributed in various cells of the central nervous system (CNS), peripheral nervous system (PNS), enteric nervous system, neuromuscular junction and immune system, which is consist of pentameric combinations of α and/or β subunits (Dani, 2015; Dani and Bertrand, 2007). Among its many subtypes, α7 nAchRs, encoded by the *Chrna7* gene, mediates systemic inflammatory homeostasis between the CNS and the immune system through a vagus nerve mediated way known as the "cholinergic anti-inflammatory pathway" (Andersson and Tracey, 2012; Lei and Duan, 2021; Martelli et al., 2014; Olofsson et al., 2012; Piovesana et al., 2021; Ulloa, 2005; Wang et al., 2003; Wu et al., 2021). We previously reported that *Chrna7* KO mice show depression-like phenotypes through systemic inflammation (Pu Y, et al., 2021b; Zhang et al., 2016b).

Increasing evidence suggests altered composition of intestinal microbiota in rodents with depressive-like phenotypes (Chang et al., 2022; Hashimoto, 2020; Huang et al., 2019; Park et al., 2013; Qu et al., 2017; Wang et al., 2020a, 2020b; Wong et al., 2016; Yang et al., 2017; 2019; Zhang et al., 2017; Zhang et al., 2019), and patients with depression (Caso et al., 2021; Jiang et al., 2015; Li et al., 2022; Nikolava et al., 2021; Sanada et al., 2020; Wei et al., 2022a; 2022b; Wong et al., 2016; Zheng et al., 2016). Fecal microbiota transplantation (FMT) of certain intestinal microbiota from depressed patients or rodents with depressive-like phenotypes causes depression-like phenotypes in mice (Kelly et al., 2016; Pu Y, et al., 2021b; 2022; Wang et al., 2020a; Yang et al., 2019; Zheng et al., 2016).

Furthermore, microbial-derived metabolites, including short-chain fatty acids (SCFAs), tryptophan-derived metabolites, bile acids and D-amino acids, could regulate a number of physiological functions such as behaviors (Bartoli et al., 2021; Chang et al., 2022; Hashimoto, 2022; Li et al., 2022; Pu J, et al., 2021a; Tran and Mohajeri, 2021; Wan et al., 2022a; 2022b). Vagus nerve is known to play a key role in the bi-directional communication between the gut microbiota and the brain (Bonaz et al., 2018; Cawthon and de La Serre, 2018; Chang et al., 2022; Cryan et al., 2019; Forsythe et al., 2014). We reported that subdiaphragmatic vagotomy (SDV) blocked the onset of depression-like behavior and altered composition of intestinal microbiota in mice after lipopolysaccharide (LPS) administration (Zhang et al., 2020). Subsequently, we reported that SDV blocked the onset of depression-like behaviors in mice after FMT from mice with depression-like behaviors (Pu Y, et al., 2021b; Wang et al., 2020a; Wang et al., 2021). Collectively, it is likely that subdiaphragmatic vagus nerve plays a key role in depression-like behaviors (Chang et al., 2022; Wei et al., 2022b). However, there are no reports showing the role of subdiaphragmatic vagus nerve in depression-like phenotypes in *Chrna7* KO mice.

The aim of present study was to evaluate whether SDV could affect depression-like phenotypes and reduced expression of synaptic proteins in the medial prefrontal cortex (mPFC) of *Chrna7* KO mice. Furthermore, we performed 16s rRNA analysis for gut microbiota composition and untargeted metabolomics analysis of plasma samples.

Materials and Methods

Animals

Mice deficient in α7 nAChR (coded by *Chrna7* gene, C57BL/6 background) were purchased from the Jackson Laboratory (Bar Harbor, ME, USA) (Zhang et al., 2016b). Adult male wild-type (WT) and *Chrna7* KO mice used in this study were littermates. All the experimental mice were aged 9 weeks, body weight 21–27 g. All the experimental mice were acclimatized to standard laboratory conditions (3 or 4/cage), maintain alternating cycles of 12 hours of light and 12 hours of darkness (lights on from 7: 00 ~ 19: 00), and under constant room temperature of 23 ± 1℃ and controlled humidity of 55 ± 5%. Animals were given free admittance to chow and water. The experimental protocol of present study

was approved by the Chiba University Institutional Animal Care and Use Committee (Permission number 3-399). The experimental mice were all firstly deeply anesthetized with inhaled isoflurane and then rapidly sacrificed by cervical dislocation. All efforts were made to minimize animals suffering.

Bilateral subdiaphragmatic vagotomy (SDV)

Bilateral SDV or sham surgery was performed under continuous inhalation anesthesia with 4-5% isoflurane by using an inhalation small animal anesthesia apparatus (KN-1071 NARCOBIT-E; Natsume Seisakusho, Tokyo, Japan), as previously method (Pu Y, et al., 2021b; Wang et al., 2020a; 2021; Zhang et al., 2020) with a slight modification. Briefly, each mouse was placed in the right-side decubitus position, the skin is disinfected with iodophor disinfectant and sterile tissue is laid. Starting from the midline alba of the abdomen, about 1 cm incision parallel to the costal arch was made at 0.5 cm below the left costal arch. The incision was gently opened with Mini incision spreader to expose the underlying liver tissue. The liver tissue was carefully pushed upward using a small sterilized cotton ball moistened with physiological saline solution and with the aid of an animal surgical microscope (Leica, Heidelberg, Germany), the fascia between the caudate lobe and the left lobe of the liver was sharply cut to fully expose the esophagus and the surrounding surgical field of view. In this case, the dorsal and ventral branches running along the esophagus under the diaphragm of the vagus nerve can be clearly identified and can be severed after careful separation. After that, no bleeding was detected, and no additional injury of esophagus, liver and other organs was checked, the liver tissue was returned to its original normal position, and 0.5 ml physiological saline solution was injected into the abdominal cavity. Then 5-0 surgical silk sutures were used to suture the abdominal incision muscle and skin layers layer by layer, ensuring aseptic operation throughout the operation. The successful implementation of SDV was confirmed by a significant increase in stomach volume on the 14th postoperative day due to loss of vagus nerve innervation.

During the sham operation, the abdominal wall incision of the same size was made in the same way at the same site. After the dorsal and ventral branches of the subdiaphragmatic vagus nerve were also softly exposed but not cut off, no bleeding and no additional damage of other organs was checked.

After the abdominal organs were restored to their normal positions, 0.5 ml normal saline was also injected into the abdominal cavity, then the incision was sutured layer by layer using the same method.

Behavioral tests

Male WT and *Chrna7* KO mice born in the same litter were subjected to behavioral tests, as previously method (Pu Y, et al., 2021b; Wang et al., 2020a; 2021). Behavioral tests including locomotion test (LMT), forced swimming test (FST), and 1% sucrose preference test (1% SPT) (Fig. 1A).

In order to monitor the locomotor activity of the mice, we adopted an automatic animal movement analysis system (SCANET MV-40; MELQUEST Co., Ltd., Toyama, Japan). The cumulative ambulatory activity counts were automatic document continuously over a total stage of 60 minutes (10 minutes × 6 times) after the mice were placed into the experimental cube boxes [33 cm (height) × 56 cm (width) × 56 cm (length)]. To avoid experimental interference, the cube boxes were cleaned up during the test interval.

A mouse automated forced-swim apparatus (SCANET MV-40; MELQUEST Co., Ltd., Toyama, Japan) was used to perform FST. Mice were placed into an inescapable transparent tank [31 cm (height) × 23 cm (diameter)] that is filled with tap water at a temperature of 23 ± 1℃ and a depth of 15 cm. Then their escape related mobility behavior was measured immediately. The immobility times were automatic document and calculated using the analytical software of the apparatus over a total stage of 6 minutes (1 minutes × 6 times).

For 1% SPT, which was carried out in the separate animal's home cage. Each mouse was presented with two dual bearing sipper bottles, one bottle contained tap water, and the second contained a 1% sucrose solution. After 24 hours of every mouse exposed to the respective two bottles containing different solution, replaced the positions of two bottles for each other to lower any confound produced by a side bias. After another 24 hours, all food and bottles were deprived lasting 4 hours, then performed 1 hour exposure to two identical bottles (containing tap water and 1% sucrose solution), which were weighed before and after the exposure period. The 1% sucrose preference was calculated as a percentage of 1% sucrose solution intake weight over the total liquid intake weight.

Western blotting analysis of synaptic proteins (PSD-95 and GluA1)

Western blotting analysis was performed as previously method (Pu Y, et al., 2021b; Wang et al., 2020a; 2021; Yang Y, et al., 2022b). The mPFC tissues were mechanical homogenized just right in ice-cold Laemmli lysis buffer. To avoid cross-contamination, each specimen was prepared separately, liquid supernatants were collected after centrifugation at 3, 000 × g (RCF) at 4℃ for 5 min. The total protein concentration extracted from each sample was detected on a spectrophotometer (Molecular Devices Emax Precision Microplate Reader; Molecular Devices., San Jose, CA, USA) using a DC protein assay kit (Bio-Rad, Hercules, CA, USA). By adding a quarter volume of sample buffer (125 mM Tris-HCl, pH 6.8; 0.1% bromophenol blue; 4% sodium dodecyl sulfate; and 10% β-mercaptoethanol and 20% glycerol) and Laemmili Lysis buffer in appropriate proportions to balance the total protein concentration of each sample, then incubate them at 95°C for 10 minutes.

Considering the size of target protein, we chose 10% sodium dodecyl sulfate–polyacrylamide gel electrophoresis (SDS-PAGE) (catalog #: 4568125, Mini-PROTEAN TGX™ Stain-Free Gels; Bio-Rad, USA) separated the proteins by gel electrophoresis. Then a Trans-Blot Mini Cell apparatus (Bio-Rad) was used to electrotransfer the target protein onto polyvinylidene difluoride membranes.

For immunodetection, the polyvinylidene difluoride membranes were blocked with blocker [5% skim milk in TBS + 0.1% Tween-20 (TBST)] at room temperature for 1 hour, the membranes for detecting postsynaptic density protein 95 (PSD-95) were incubated with the recommended dilution of the primary antibody against PSD-95 (1: 1, 000, Catalog No.: 51-6900, 1 μg/mL, Invitrogen, Camarillo, CA, USA) and β-actin (1: 10, 000; Cat number: A5441 Sigma-Aldrich Co., Ltd, St Louis, MO, USA) at 4°C overnight. The next day, wash the polyvinylidene difluoride membranes in three washes of TBST, 10 minutes each. Then the polyvinylidene difluoride membranes were selectively incubated with a recommended dilution of labeled secondary antibody [anti-mouse antibody (1: 5, 000, catalog No.: NA931, GE Healthcare) or a horseradish peroxidase-conjugated anti-rabbit antibody (1: 5, 000, catalog No.: NA934, GE Healthcare)] in 5% blocking buffer in TBST at room temperature for 1 hour. After three final washes in TBST, 10 minutes each. The bands in the polyvinylidene difluoride

membranes were detected using enhanced chemiluminescence plus a Western Blotting Detection system (GE Healthcare Bioscience).

The membranes for detecting anti-glutamate receptor 1 (AMPA subtype: GluA1) were incubated in elution buffer (62.5 mM Tris–HCl, pH 6.8, 2% sodium dodecyl sulfate, and 100 mM β-mercaptoethanol) (preheat in incubator at 60° C for 10 minutes, shake 50 times/min) at 60°C for 30 minutes and then washed three times (10 minutes at a time) in TBST. The stripped membranes were blocked with blocker [5% skim milk in TBS + 0.1% Tween-20 (TBST)] at room temperature for 1 hour and then were incubated with the recommended dilution of primary antibody directed against GluA1 (1: 1, 000; Cat No.: ab31232, Abcam, Cambridge, MA, USA) at 4° C overnight. The following day, washing the membranes for three times (10 minutes at a time) in TBST and were incubated with a recommended dilution of horseradish peroxidase-conjugated anti-rabbit antibody (1: 5, 000, catalog No.: NA934, GE Healthcare) for 1 hour at room temperature. After three final washes in TBST, 10 minutes each. The bands in the polyvinylidene difluoride membranes were detected using enhanced chemiluminescence plus a Western Blotting Detection system (GE Healthcare Bioscience). Images were produced using a ChemiDoc™ Touch Imaging System (170-01401; Bio-Rad Laboratories, Hercules, CA, USA), and immunoreactive bands were quantified using Image Lab^{TM}3.0 software (Bio-Rad Laboratories).

Collection of fresh fecal samples and 16S ribosome RNA sequencing

We collected fresh fecal samples from mice before behavioral test LMT (Fig. 1A). To avoid cross-contamination, fecal samples from each mouse were collected separately. After the mice defecated, fresh fecal samples were collected immediately and were quickly intromitted into individual sterilized screw cap microtubes and then were stored at -80℃ until use.

Extraction of total DNA from mouse feces samples and subsequent 16S rRNA analysis were performed at MyMetagenome Co., Ltd. (Tokyo, Japan). The specific operation scheme can be carried out according to the procedure previously reported (Pu Y, et al., 2021b; Wang et al., 2020a; 2021; Yang Y, et al., 2022b). In brief, in order to amplify the V1-V2 hypervariable region of the bacterial 16S

ribosome RNA gene, the universal primers 27F-mod (5′-AGRGTTTGATYMTGGCTCAG-3′) and 338R (5′-TGCTGCCTCCCGTAGGAGT-3′) have been used in the process of PCR. Then used an Illumina MiSeq Platform to sequence the 16S amplicons. The similarities between the genome database of the National Center for Biotechnology Information (NCBI) and the Ribosome Database Project were searched by using the GLSEARCH program. Finally, OTUs were classified and identified. α-diversity analysis such as Observed_otus, Chao1, Ace, Shannon, and Shannon_e was used to reflect the abundance and diversity of intestinal microbial communities. β-diversity analysis including Principal Co-ordinates Analysis (PCoA) was used to access similarity or dissimilarity of the three intestinal microbial communities. Linear discriminant analysis (LDA) effect size (LEfSe) was used for identifying certain bacteria as potential microbial biomarkers discovery. Microbiota-based potential biomarker discoveries were performed with LEfSe using the online galaxy platform (Segata et al., 2011). The LDA scores ($LDA > 4.0$ and $P < 0.05$) derived from LEfSe analysis were considered significantly to be enriched or deficient bacterial taxa in the intestinal microbiota among the three groups.

Untargeted metabolomics analysis of plasma samples and data preprocessing

Untargeted metabolomics profiles from plasm samples were analysis by using ultra-performance liquid chromatography-tandem quadruple time-of-flight mass spectrometry (UPLC-QTOF/MS) technique. The acquisition was operated on an ExionLC™ AD system (SCIEX, Tokyo, Japan) coupled to a X500R QTOF system (SCIEX, Tokyo, Japan), as previously reported (Wan et al., 2022a; 2022b). With the help of R statistical environment Ver 4.0.5. and Mass Spectrometry-Data Independent AnaLysis (MS-DIAL) software version 4.60 (Tsugawa et al., 2015), metabolomics profiles data was analyzed. Metabolites were detected at least 50% from the analyzed samples and the coefficient of variation (CV) values of 30% of metabolites in pooled quality control (QC) samples, and annotation level 2 proposed by Schymanski et al. (2014) were used for data analysis.

Statistical analysis

Statistical analysis of the data was performed using SPSS version 20.0 software (SPSS, Tokyo, Japan).

The data were shown as the mean ± standard error of the mean (S.E.M.). Data for behavioral tests and the expression levels of synaptic proteins were analyzed using one-way analysis of variance (ANOVA), followed by Fisher's least significant difference (LSD) test. The data of body weight were analyzed using repeated measure ANOVA, followed by Fisher's LSD test. Metabolites, the α-diversity of intestinal microbiota, and the abundance of gut microbiota at the phylum level, genus level, and species level among the three groups were analyzed using the Kruskal-Wallis test, followed by the Dunn's test for post-hoc analysis. Pairwise comparison of metabolomics data among the three groups were analyzed by Wilcoxon rank sum test. Bioinformatic analysis of PCoA, LEfSe algorithm of intestinal microbiota, Volcanic plot analysis of metabolomics and Correlation networks were all performed by using the OmicStudio tools (https://www.omicstudio.cn/tool).

Correlations between the plasma metabolites and the intestinal microbiota at species level, depression-like phenotypes and the expression of synaptic proteins in the brain, and correlations between the relative abundance of species bacteria and the expression levels of synaptic proteins in the mPFC and depression-like phenotypes were analyzed using Spearman's correlation analysis. P-value for comparison less than 0.05 was regarded as significant.

Results

Effects of bilateral SDV on depression-like phenotypes, and the expression of synaptic proteins in the brain

Effects of bilateral SDV in depression-like phenotypes in *Chrna7* KO mice were investigated (Fig. 1A). Body weight after surgery was not different among the three groups (Fig. 1B). There were no changes in locomotion among the three groups (Fig. 1C). The immobility time of FST in the KO + sham group was significantly higher than that of WT + sham group and KO + SDV group (Fig. 1D). In the SPT, sucrose preference of KO + sham group was significantly lower than that of WT + sham and KO + SDV groups (Fig. 1E). There were no differences in FST immobility time and sucrose preference of SPT between WT + sham group and KO + SDV group (Fig. 1D and 1E).

It is well known that synaptic proteins such as PSD-95 and GluA1 are decreased in the mPFC of

rodents with depression-like phenotypes (Pu Y, et al., 2021b; Wang et al., 2020a; 2020b; 2021; Yang et al., 2015; Zhang et al., 2014). Western blotting analysis showed that the expressions of PSD-95 and GluA1 in the mPFC of the KO + sham group were significantly lower than those of WT + sham group and KO + SDV group (Fig. 1F and 1G). There were no differences in expressions of GluA1 and PSD-95 in the mPFC between WT + sham group and KO + SDV group (Fig. 1F and 1G).

These data suggest that bilateral SDV significantly blocked depression-like phenotypes and reduced expression of synaptic proteins in the mPFC of *Chrna7* KO mice.

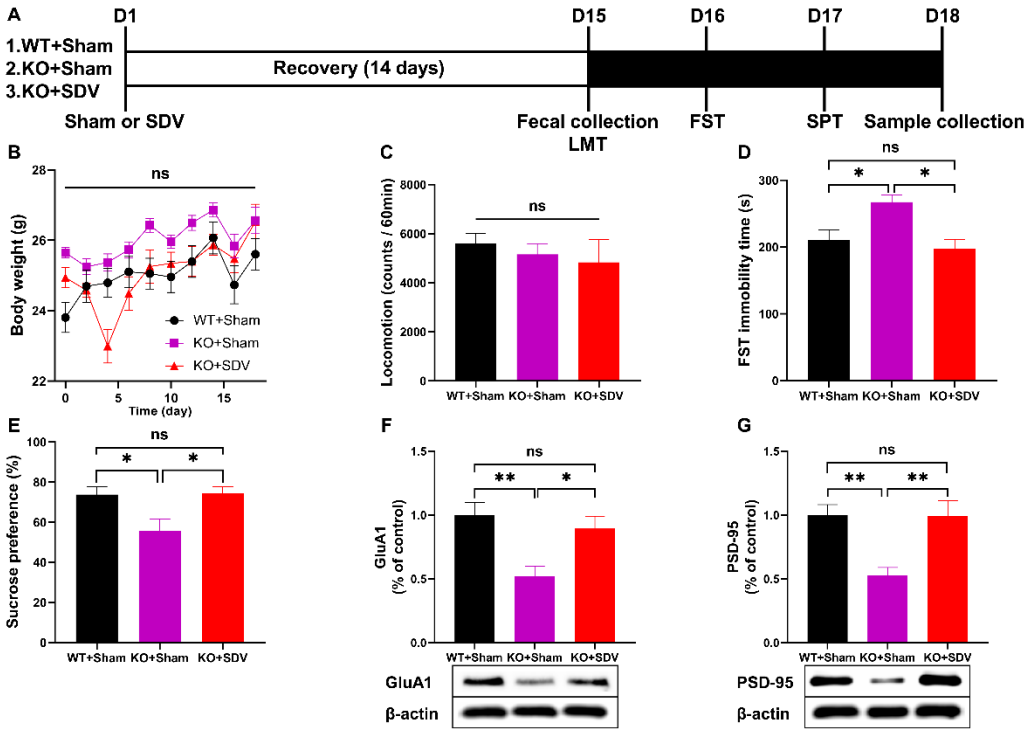

Figure 1. Effects of bilateral SDV on depression-like phenotypes and reduced expression of synaptic proteins in *Chrna7* KO mice

(A): Experimental schedule. On day 1, bilateral SDV or sham was performed, and they were recovered 14 days. On day 15, fresh feces samples were collected, and subsequently LMT was performed. FST and SPT were performed on day 16 and day 17, respectively. On day 18, medial prefrontal cortex (mPFC) and plasma samples were collected. (B): Body weight (repeated measure ANOVA, $F(2, 21) = 2.424$, $P = 0.1129$). (C): LMT (one-way ANOVA, $F(2, 21) = 0.4278$, $P = 0.6575$). (D): FST (one-way ANOVA, $F(2, 21) = 6.050$, $P = 0.0084$). (E): SPT (one-way ANOVA, $F(2, 21) = 5.312$, $P = 0.0136$). (F): Western blot analysis of GluA1 in the mPFC (one-way ANOVA, $F(2, 21) = 6.805$, $P = 0.0053$) and the representative bands. (G): Western blot analysis of PSD-95 in the mPFC (one-way ANOVA, $F(2, 21) = 8.191$, $P = 0.0023$) and the representative bands. The data are shown as means ± S.E.M (WT + sham group: n = 10, KO + sham group: n = 7, KO + SDV group: n = 7). ANOVA: analysis of variance. ns: not significant; *$P < 0.05$; **$P < 0.01$; ***$P < 0.001$.

Effects of bilateral SDV on the composition diversity of intestinal microbiota

For α-diversity, Kruskal-Wallis test revealed no statistically significant differences in the Observed_otus, Chao1, Ace, Shannon, and Shannon_e indices among the three group (Fig. 2A-2E). Regarding β-diversity, the bacterial population composition of intestine microbiota in the three groups was analyzed by PCoA. Based on the OUT level, PCoA analysis showed a significant separation in the bacterial population composition through Analysis of similarities (ANOSIM) assessment (R = 0.3500, P = 0.001) (Fig. 2F).

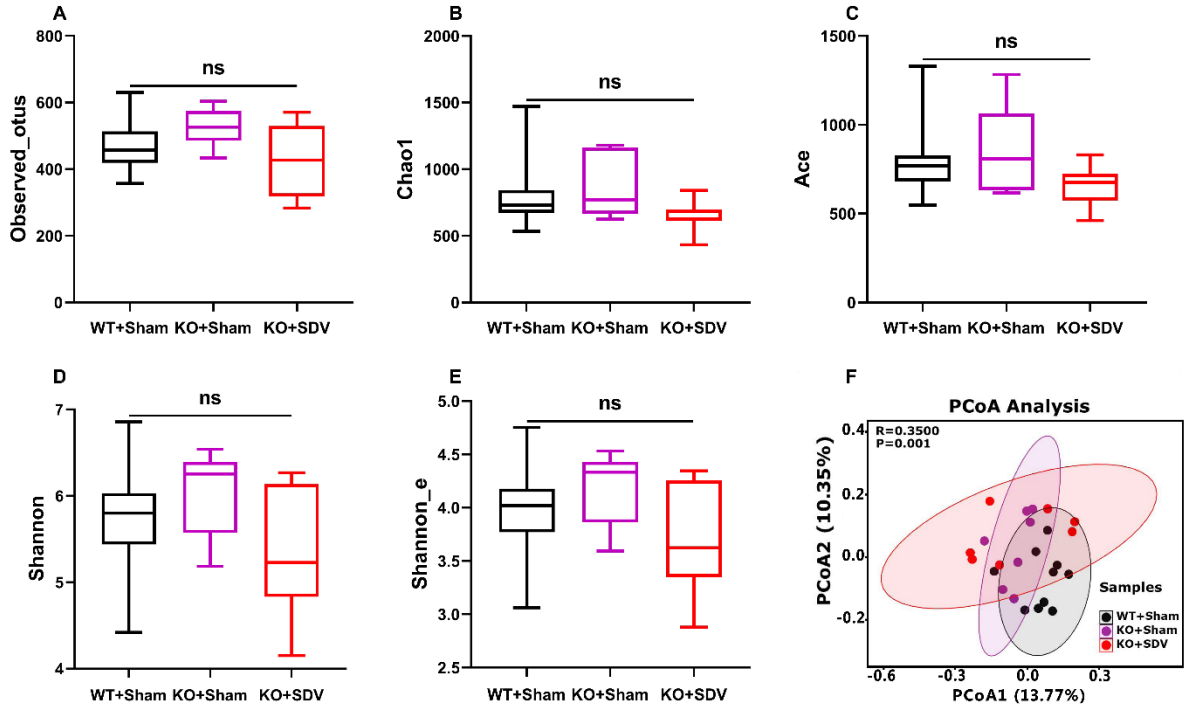

Figure 2. Effects of bilateral SDV on the diversity of gut microbiota composition

(A): Observed_otus (Kruskal-Wallis test, P = 0.2028). (B): Chao1 (Kruskal-Wallis test, P = 0.1920). (C): Ace (Kruskal-Wallis test, P = 0.2305). (D): Shannon (Kruskal-Wallis test, P = 0.1941). (E): Shannon_e (Kruskal-Wallis test, P = 0.1941). (F): PCoA based on OTU level (ANOSIM, Bray-Curtis dissimilarity matrix) (R = 0.3500, P = 0.001). For all box plots, the middle line in the box addresses the median, the box addresses the interquartile range, and the whisker addresses the most extreme and least values. ns: not significant.

Effects of bilateral SDV on the LEfSe algorithm of intestinal microbiota

Cladogram presented the relationship between biomarker taxa (layers of the cladogram represent different levels, with phylum, class, order, family, genus, and species from inside to outside)

generated by LEfSe analysis (Fig. 3A). Furthermore, we identified 5 taxonomic biomarkers, the species *Porphyromonadaceae bacteriumC941*, the genus *G_undefined_Porphyromonadaceae*, the species *Gabonibacter massiliensis*, the genus *Gabonibacter*, and the species *Prevotella sp. oral taxon 317* for the WT + sham group. Furthermore, we identified 6 taxonomic biomarkers, the species *Gabonia massiliensis*, the genus *Gabonia*, the family *Porphyromonadaceae*, the order *Bacteroidales*, the class *Bacteroidia*, and the phylum *Bacteroidetes* for the KO + sham group. Moreover, we identified 8 taxonomic biomarkers, the species *Lactobacillus hominis*, the species *Lactobacillus reuteri*, the species *Lactobacillus sp. BL302*, the genus *Lactobacillus*, the family *Lactobacillaceae*, the order *Lactobacillales*, the class *Bacilli*, and the *phylum Firmicutes* for the KO + SDV group (Fig. 3B).

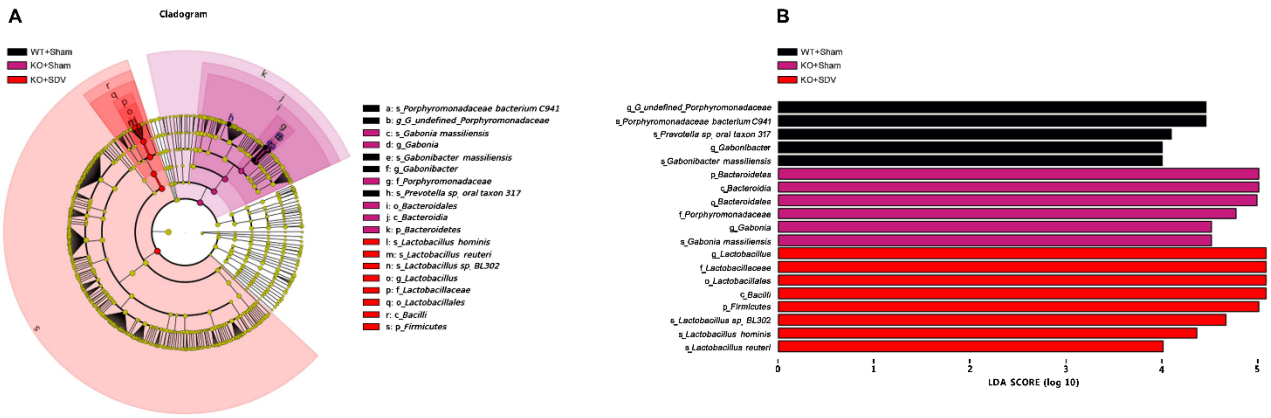

Figure 3. LEfSe analysis for potential bacteria biomarkers of gut microbiota

(A): Functional branching diagram generated from LEfSe showing the differences of the three groups at different taxonomic levels. (B): Histogram representing the enriched taxa with LDA score > 4.0 and P < 0.05 obtained from LEfSe of the three groups.

Effects of bilateral SDV on the intestinal microbiota at the levels of phylum, genus, and species

At the phylum level, the composition of the intestinal microbiota in *Chrna7* KO mice was altered after SDV (Fig. 4A). Compared with WT + sham group and KO + sham group, the relative abundance of *Firmicutes* in the KO + SDV group were significantly higher, although there were no significant differences between WT + sham group and KO + sham group (Fig. 4B). Although there were no significant differences in the relative abundance of *Tenericutes* between KO + SDV group and KO + sham group, the relative abundance of *Tenericutes* in the KO + SDV group were significantly lower than that in the WT + sham group (Fig. 4C).

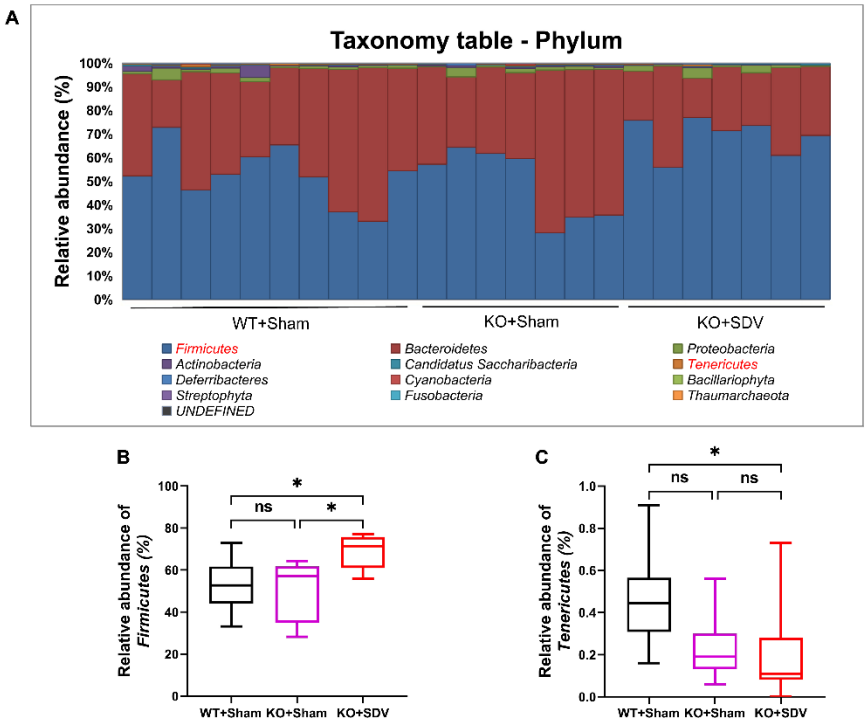

Figure 4. Effects of bilateral SDV on gut microbiota at the phylum levels

(A): Gut bacteria composition at the phylum level in the three groups. (B): Relative abundance of the phylum *Firmicutes* (Kruskal-Wallis test, P = 0.0126). (C): Relative abundance of the phylum *Tenericutes* (Kruskal-Wallis test, P = 0.0258). For all box plots, the middle line in the box addresses the median, the box addresses the interquartile range, and the whisker addresses the most extreme and least values. *P < 0.05. ns: not significant.

At the genus level, the composition of the gut microbiota in *Chrna7* KO mice was altered after SDV (Fig. 5A). The relative abundance of *Faecalibaculum* in the KO + SDV group were statistically significantly lower than in the WT + sham group and KO + sham group (Fig. 5B). The relative

abundance of *Candidatus Arthromitus*, *Bifidobacterium*, *G_undefined_Burkholderiales*, and *Muribaculum* in the KO + SDV group was lower than that in the WT + sham group, whereas the relative abundance of *Ihubacter* in the KO + SDV group was higher than that in the WT + sham group (Fig. 5C, 5F, and 5I-5J). The relative abundance of *Turicibacter* in the KO + SDV group were lower than in the KO + sham group (Fig. 5D). The relative abundance of *Lactobacillus* in the KO + SDV group were higher than in the KO + sham group (Fig. 5G). The relative abundance of *Lactococcus* in the KO + sham group and the KO + SDV group were lower than the WT + sham group (Fig. 5E).

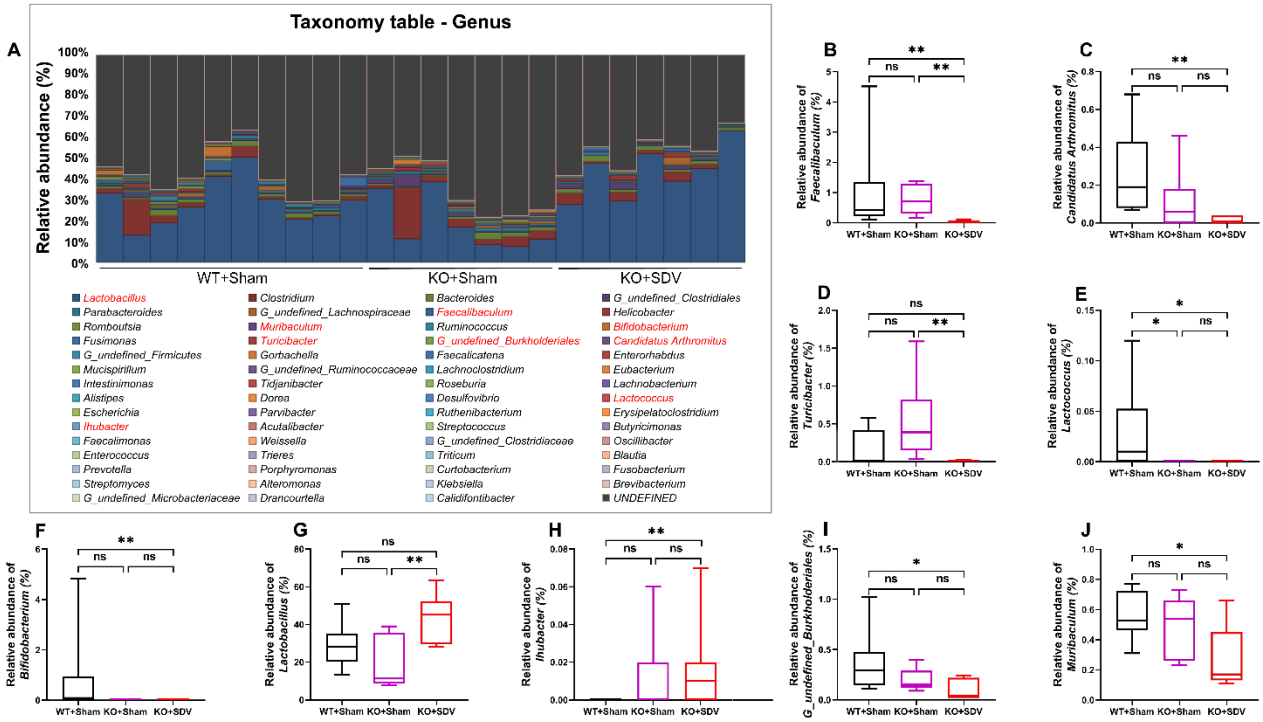

Figure 5. Effects of bilateral SDV on gut microbiota at the genus levels

(A): Gut bacteria composition at the genus level in the three groups. (B): Relative abundance of the genus *Faecalibaculum* (Kruskal-Wallis test, P = 0.0009). (C): Relative abundance of the genus *Candidatus Arthromitus* (Kruskal-Wallis test, P = 0.0021). (D): Relative abundance of the genus *Turicibacter* (Kruskal-Wallis test, P = 0.0030). (E): Relative abundance of the genus *Lactococcus* (Kruskal-Wallis test, P = 0.0053). (F): Relative abundance of the genus *Bifidobacterium* (Kruskal-Wallis test, P = 0.0086). (G): Relative abundance of the genus *Lactobacillus* (Kruskal-Wallis test, P = 0.0102). (H): Relative abundance of the genus *Ihubacter* (Kruskal-Wallis test, P = 0.0131). (I): Relative abundance of the genus *G_undefined_Burkholderiales* (Kruskal-Wallis test, P = 0.0132). (J): Relative abundance of the genus *Muribaculum* (Kruskal-Wallis test, P = 0.0395). For all box plots, the middle line in the box addresses the median, the box addresses the interquartile range, and the whisker addresses the most extreme and least values. *P < 0.05; **P < 0.01. ns: not significant.

At the species level, we screened out 15 bacteria with statistical differences based on their relative abundance (Fig. 6A). There were significant differences in the relative abundance of *Lactobacillus intestinalis*, *Lactobacillus hominis*, *Faecalibaculum rodentium*, *Lactobacillus sp. BL302*, *Bacteroides sp. TP-5*, *Candidatus Arthromitus sp. SFB-mouse*, *Turicibacter sp. LA62*, *Lactobacillus reuteri*, *Lactococcus lactis*, *Lactobacillus sp. NBRC 14512*, *Clostridium sp. Culture Jar-56*, *Lachnospiraceae bacterium 607*, *Clostridiales bacterium CIEAF 030*, *Bifidobacterium pseudolongum* and *Muribaculum intestinale* (Fig. 6B-6P). Among these microbes, the relative abundance of three microbiome (*Lactobacillus intestinalis*, *Lactobacillus sp. BL302*, *Turicibacter sp. LA62*) was significantly different between KO + sham group and KO + SDV group (Fig. 6B, 6E, and 6H).

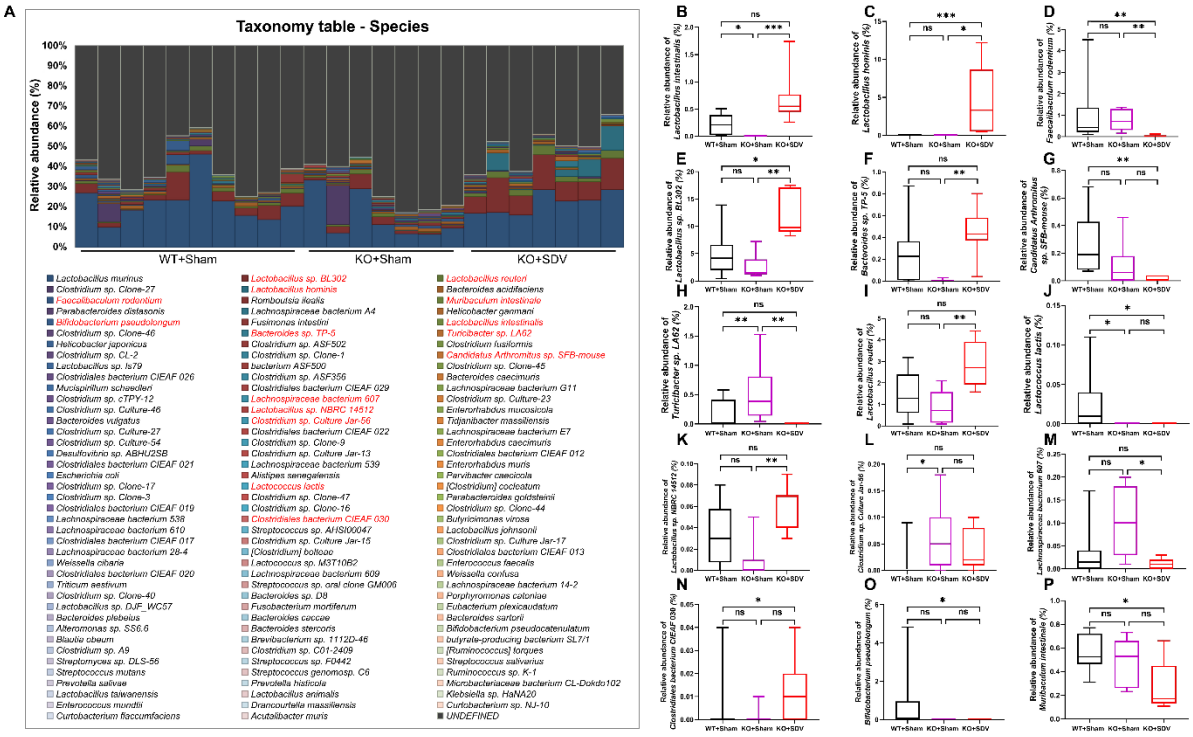

Figure 6. Effects of bilateral SDV on gut microbiota at the species levels

(A): Gut bacteria composition at the species level in the three groups. (B): Relative abundance of the species *Lactobacillus intestinalis* (Kruskal-Wallis test, P = 0.0001). (C): Relative abundance of the species *Lactobacillus hominis* (Kruskal-Wallis test, P = 0.0002). (D): Relative abundance of the species *Faecalibaculum rodentium* (Kruskal-Wallis test, P = 0.0009). (E): Relative abundance of the species *Lactobacillus sp. BL302* (Kruskal-Wallis test, P = 0.0012). (F): Relative abundance of the species *Bacteroides sp. TP-5* (Kruskal-Wallis test, P = 0.0018). (G): Relative abundance of the species *Candidatus Arthromitus sp. SFB-mouse* (Kruskal-Wallis test, P = 0.0023). (H): Relative abundance of the species *Turicibacter sp. LA62* (Kruskal-Wallis test, P = 0.0030). (I): Relative abundance of the species *Lactobacillus reuteri* (Kruskal-Wallis test, P = 0.0047). (J): Relative abundance of the species

Lactococcus lactis (Kruskal-Wallis test, P = 0.0053). (K): Relative abundance of the species *Lactobacillus sp. NBRC 14512* (Kruskal-Wallis test, P = 0.0088). (L): Relative abundance of the species *Clostridium sp. Culture Jar-56* (Kruskal-Wallis test, P = 0.0155). (M): Relative abundance of the species *Lachnospiraceae bacterium 607* (Kruskal-Wallis test, P = 0.0155). (N): Relative abundance of the species *Clostridiales bacterium CIEAF 030* (Kruskal-Wallis test, P = 0.0214). (O): Relative abundance of the species *Bifidobacterium pseudolongum* (Kruskal-Wallis test, P = 0.0245). (P): Relative abundance of the species *Muribaculum intestinale* (Kruskal-Wallis test, P = 0.0395). For all box plots, the middle line in the box addresses the median, the box addresses the interquartile range, and the whisker addresses the most extreme and least values. *P < 0.05; **P < 0.01; ***P < 0.001. ns: not significant.

Untargeted metabolomic profiles analysis of plasma samples

Considering the close interaction between intestinal microbiome and host metabolism, we conducted untargeted metabolomics profiles analysis from plasma samples. After the quality control and removal of low-abundance peaks, a subset of 175 metabolites was annotated. After log10 transformation of the concentration of metabolomics data, Kruskal-Wallis test was performed among the three groups. We identified 24 metabolites with statistical differences (Fig. 7A-7D).

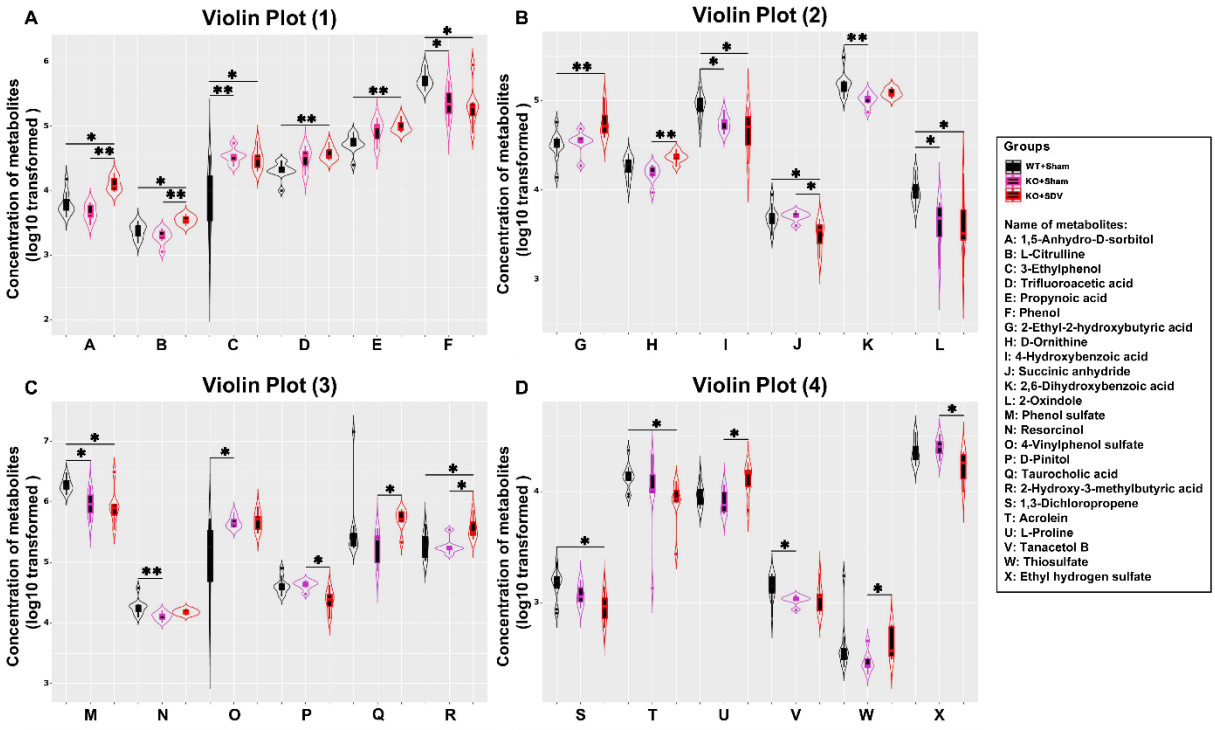

Figure 7. Effect of bilateral SDV on plasma metabolites

(A): Violin plot showing the changes of 6 kinds of metabolites [1,5-anhydro-D-sorbitol (Kruskal-Wallis test, P = 0.0016), L-citrulline (Kruskal-Wallis test, P = 0.0018), 3-ethylphenol (Kruskal-Wallis test, P = 0.0019), trifluoroacetic acid (Kruskal-Wallis test, P = 0.0046), propynoic acid (Kruskal-Wallis test, P = 0.0046), phenol (Kruskal-Wallis test,

P = 0.0055)] among the three groups. (B): Violin plot showing the changes of 6 kinds of metabolites [2-ethyl-2-hydroxybutyric acid (Kruskal-Wallis test, P = 0.0059), D-ornithine (Kruskal-Wallis test, P = 0.0065), 4-hydroxybenzoic acid (Kruskal-Wallis test, P = 0.0077), succinic anhydride (Kruskal-Wallis test, P = 0.0078), 2,6-dihydroxybenzoic acid (Kruskal-Wallis test, P = 0.0080), 2-oxindole (Kruskal-Wallis test, P = 0.0080)] among the three groups. (C): Violin plot showing the changes of 6 kinds of metabolites [phenol sulfate (Kruskal-Wallis test, P = 0.0080), resorcinol (Kruskal-Wallis test, P = 0.0111), 4-vinylphenol sulfate (Kruskal-Wallis test, P = 0.0113), D-pinitol (Kruskal-Wallis test, P = 0.0122), taurocholic acid (Kruskal-Wallis test, P = 0.0129), 2-hydroxy-3-methylbutyric acid (Kruskal-Wallis test, P = 0.0145)] among the three groups. (D): Violin plot showing the changes of 6 kinds of metabolites [1,3-dichloropropene (Kruskal-Wallis test, P = 0.0203), acrolein (Kruskal-Wallis test, P = 0.0209), L-proline (Kruskal-Wallis test, P = 0.0245), tanacetol B (Kruskal-Wallis test, P = 0.0321), thiosulfate (Kruskal-Wallis test, P = 0.0436), ethyl hydrogen sulfate (Kruskal-Wallis test, P = 0.0460)] among the three groups. The X-axis using the letter symbol representing the names of different plasma metabolites, and the Y-axis represents the concentration of various plasma metabolites after log10 transformation. *P < 0.05; **P < 0.01; Different colors of violin plots represent the corresponding groups.

Then we conducted pairwise comparison of metabolomics data among the three groups, and screened out the metabolites with significant up-regulation and down-regulation obtained in each two groups through the form of Volcano plot [the threshold was set as: $P < 0.05$ and fold change (FC) > 2]. When comparing the WT + sham group with the KO + sham group, we confirmed that 3 annotation metabolites were significantly up-regulated and 7 annotation metabolites were significantly down-regulated (Fig. 8A). When comparing the WT + sham group with the KO + SDV group, we confirmed that 9 annotation metabolites were significantly up-regulated and 8 annotation metabolites were significantly down-regulated (Fig. 8B). When the KO + sham group compared with the KO + SDV group, we confirmed 9 significantly up-regulated annotated metabolites and 4 significantly down-regulated metabolites (Fig. 8C).

Finally, we further used UpSet plot listed out that there were 11 kinds of annotated metabolites with statistical differences between WT + sham group and KO + sham group, 17 kinds of annotated metabolites with statistical differences between the KO + sham group and KO + SDV group, and 27 kinds of annotated metabolites with statistical differences between WT + sham group and KO + SDV group. In addition, 6 kinds of annotated metabolites showed significant differences between the WT + sham group and the KO + sham group, and between the WT + sham group and the KO + SDV group. Furthermore, 9 kinds of annotated metabolites showed significant differences between the KO + sham group and the KO + SDV group, and between the WT + sham group and the KO + SDV group (Fig. 8D).

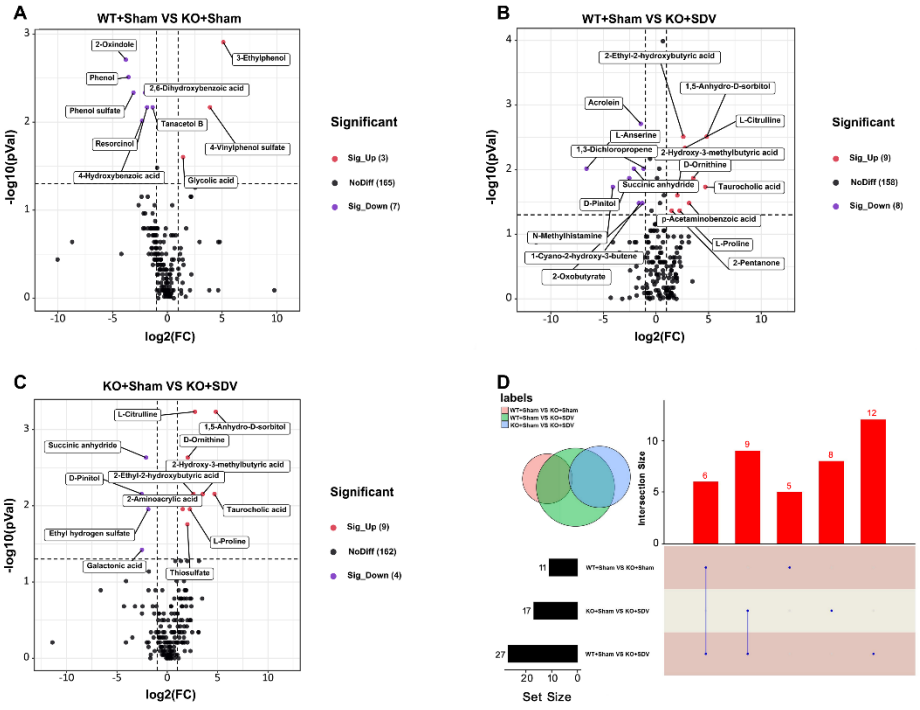

Figure 8. Differences of plasma metabolites between different experimental groups

(A): Volcano plot indicating 3 annotation metabolites were significantly up-regulated, 7 annotation metabolites were significantly down-regulated and 165 annotation metabolites were no differences when comparing the WT + sham group with the KO + sham group. (B): Volcano plot indicating 9 annotation metabolites were significantly up-regulated, 8 annotation metabolites were significantly down-regulated and 158 annotation metabolites were no differences when comparing the WT + sham group with the KO + SDV group. (C): Volcano plot indicating 9 annotation metabolites were significantly up-regulated, 4 annotation metabolites were significantly down-regulated and 162 annotation metabolites were no differences when comparing the KO + sham group with the KO + SDV group. The X-axis represents the log2-transformed values of the FC of plasma metabolite concentration, and the Y-axis represents the -log10-transformed values of P value using the Wilcoxon rank sum test. The horizontal dotted line indicates P = 0.05 and the vertical dotted line indicates FC = ± 2. Metabolites with up-regulated, down-regulated, and no difference were marked in red, purple, and black respectively. (D): UpSet plot listed out there were 11 kinds of annotated metabolites with statistical differences between the WT + sham group and the KO + sham group, 17 kinds of annotated metabolites with statistical differences between the KO + sham group and the KO + SDV group, and 27 kinds of annotated metabolites with statistical differences between the WT + sham group and the KO + SDV group by using the Wilcoxon rank sum test ($P < 0.05$). In addition, 6 kinds of annotated metabolites showed significant differences between the WT + Sham group and the KO + sham group and between the WT + sham group and the KO + SDV group, and 9 kinds of annotated metabolites showed significant differences between the KO + sham group and the KO + SDV group and between the WT + sham group and the KO + SDV group. Besides, 5 kinds of annotated metabolites showed significant differences between the WT + sham group and the KO + sham group, 8 kinds of annotated metabolites showed significant differences between the KO + sham group and the KO + SDV group, 12 kinds of annotated metabolites showed significant differences between the WT + sham group and the KO+SDV group.

Correlations between the gut microbiota and plasma metabolites (or FST, synapse proteins)

There was a widely correlation between the plasma metabolites and the gut microbiota of the three groups, indicating the existence of a close relationship between the plasma metabolites and the gut microbiota. Furthermore, we evaluated the association between plasma metabolites and the gut microbiota at the species level. After screening the data by setting the threshold of $P < 0.05$ and the absolute value of $R \geq 0.5$, a Correlation Network was developed to indicate the correlation between the plasma metabolites and the intestinal microbiota at species level, depression-like phenotypes and the expression of synaptic proteins in the brain, all of which significantly differences among the three groups in the present study (Fig. 9A).

Two differentially relative abundant of gut bacteria (*Lactobacillus intestinalis* and *Bacteroides sp. TP-5*) were positively correlated with 1,5-anhydro-D-sorbitol (Fig. 9A). Three differentially relative abundant of gut bacteria (*Faecalibaculum rodentium*, *Turicibacter sp. LA62* and *Muribaculum intestinale*) were negatively correlated with 1,5-anhydro-D-sorbitol (Fig. 9A). There were positive correlations between the relative abundance of species *Lactobacillus intestinalis*, *Lactobacillus hominis*, *Lactobacillus sp. BL302*, *Lactobacillus sp. NBRC 14512*, and *Clostridiales bacterium CIEAF 030* and L-citrulline. In contrast, there were negative correlations between the relative abundance of species *Faecalibaculum rodentium* and L-citrulline (Fig. 9A).

The relative abundance of species *Lachnospiraceae bacterium 607* was positively correlated with succinic anhydride while the relative abundances of species *Lactobacillus hominis*, *Lactobacillus sp. BL302*, *Bacteroides sp. TP-5*, *Lactobacillus reuteri*, and *Clostridiales bacterium CIEAF 030* were negatively correlated with succinic anhydride (Fig. 9A). The species *Lactobacillus intestinalis*, *Lactobacillus hominis*, *Lactobacillus sp. BL302*, *Lactobacillus reuteri* and *Lactobacillus sp. NBRC 14512* were positively correlated with taurocholic acid. In contrast, the species *Faecalibaculum rodentium* and *Turicibacter sp. LA62* were negatively correlated with taurocholic acid (Fig. 9A).

There was only a significant positive correlation between the FST data and the concentration of ethyl hydrogen sulfate (Fig. 9A). There was no correlation between changes in SPT and changes in

metabolite concentration (data not shown). There was a positive correlation between GluA1 expression levels in mPFC and the concentration of 2-oxindole (Fig. 9A). Furthermore, there were positive correlations between PSD-95 expression levels in mPFC and the concentration of L-citrulline, D-ornithine, 2,6-dihydroxybenzoic acid or resorcinol. In contrast, there were no negative correlations between expressions of GluA1 and PSD-95 in the mPFC and plasma metabolites (Fig. 9A).

Similarly, we used a Correlation Network to investigate correlations between the relative abundance of the gut bacteria that differed significantly at the species levels among the three groups and depression-like phenotypes or the expression of synaptic proteins (Fig. 9B). After screening the data by setting the threshold of $P < 0.05$ and the absolute value of $R \geq 0.5$. There were significant negative correlations between the FST data and the relative abundance of the species *Lactobacillus intestinalis*, *Lactobacillus sp. BL302*, *Bacteroides sp. TP-5*, and *Lactobacillus sp. NBRC 14512* in the three groups (Fig. 9B), suggesting a role of these species in behavioral despair. There were statistically significant positive correlations between the SPT data and the relative abundance of species *Bacteroides sp. TP-5* in the three experimental groups (Fig. 9B), suggesting a role of *Bacteroides sp. TP-5* in anhedonia-like behavior. Furthermore, there were positive or negative correlation between expression levels of synaptic proteins in the mPFC and the relative abundance of species bacteria (Fig. 9B).

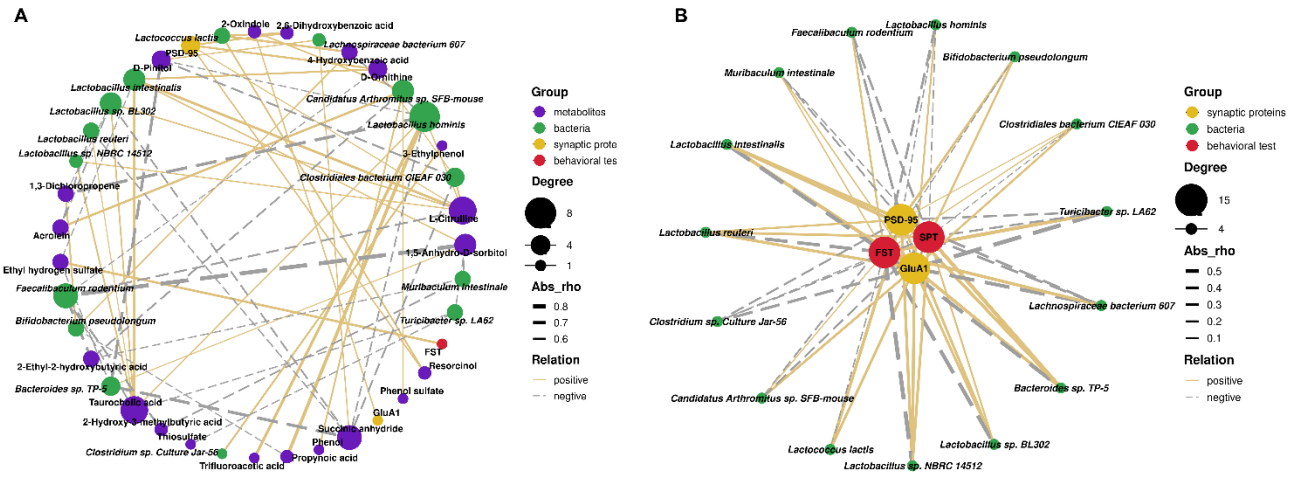

Figure 9. Correlation network between behavioral data (or synaptic proteins) and microbiota (or metabolites)

(A): A Correlation Network indicating the correlations between the concentrations of plasma metabolites and the gut microbiota at the species level, the results of the behavioral test and the expression of synaptic proteins of mPFC (The threshold was set as $P < 0.05$ and the absolute value of $R \geq 0.5$. The different colors of nodes represent different groups. The sizes of node gradients represent varying degrees of correlation. The thickness of the line represents the absolute value of the correlation coefficient. Solid lines represent positive correlations, dotted lines represent negative correlations). (B): A Correlation Network showed correlations between the relative abundance of gut bacteria at the species level and the results of the behavioral test and the expression of synaptic proteins of mPFC (The threshold was set as $P < 0.05$. The different colors of nodes represent different groups. The sizes of node gradients represent varying degrees of correlation. The thickness of the line represents the absolute value of the correlation coefficient. Solid lines represent positive correlations, dotted lines represent negative correlations).

Discussion

The major findings of this study are as follows: First, SDV blocked depression-like behaviors and reduced expression of synaptic proteins (i.e., GluA1 and PSD-95) in the mPFC of *Chrna7* KO mice. Second, there were no changes in α-diversity among the three groups. However, there was a significant difference in β-diversity among the three groups. LEfSe analysis revealed that the species *Lactobacillus sp. BL302*, the *species Lactobacillus hominis*, and the species *Lactobacillus reuteri*, were

identified as potential microbial markers in the KO + SDV group. Furthermore, there were several genus and species altered among the three groups. Third, there were several metabolites altered among the three groups. Fourth, there were correlations between relative abundance of several microbiome and behavioral data (or synaptic proteins). Network analysis showed correlations between several microbiome and blood metabolites or behavioral data. Collectively, these data suggest that subdiaphragmatic vagus nerve plays a crucial role in depression-like phenotypes in *Chrna7* KO mice through gut–microbiota– brain axis including microbiome-derived metabolites.

β-diversity data among the three groups suggest that SDV is a driving factor for the differential expression of structural similarity in microbial communities. We reported that LPS significantly decreased α-diversity and relative abundance of gut microbiota in mice, and that SDV did not cause LPS-induced alterations in α-diversity and relative abundance of gut microbiota in mice (Zhang et al., 2020), suggesting that LPS could cause depression-like behaviors in mice through gut–microbiota–brain axis via subdiaphragmatic vagus nerve. Furthermore, SDV blocked depression-like behaviors in mice after FMT from mice with depression-like behaviors (Pu Y, et al., 2021b; Wang et al., 2020a; Wang et al., 2021). McVey Neufeld et al. (2019) reported that oral treatment with selective serotonin reuptake inhibitor (SSRI: fluoxetine or sertraline) leads to a significant increase in vagal fiber activity, and that blocking vagal signaling from the gut to the brain via SDV abolished antidepressant-like effect of SSRI, suggesting the role of vagus nerve dependent gut–brain axis in the antidepressant effects of SSRIs. From the current data, it is unclear whether subdiaphragmatic vagus nerve is responsible for depression-like phenotypes of *Chrna7* KO mice. A recent study demonstrated that SDV or genetic knock-out of α7 nAchRs abolished the anti-inflammatory actions of famotidine (a histamine 2 receptor antagonist) in mice with LPS-treated cytokine stream (Yang H, et al., 2022a), suggesting a role of vagus nerve anti-inflammation via α7 nAchRs. Given the crucial role of α7 nAchRs on vagus nerve inflammatory actions (O'Mahony et al., 2009; Yang H, et al., 2022a), it is possible that subdiaphragmatic vagus nerve may be responsible for depression-like phenotypes of *Chrna7* KO mice. Taken together, it is likely that gut–microbiota–brain axis via subdiaphragmatic vagus nerve plays an

important role in depression-like phenotypes of *Chrna7* KO mice.

At the phylum level, the most abundant phylum *Firmicutes* was significantly increased in KO + SDV group compared to other two groups, suggesting that subdiaphragmatic vagus nerve may affect relative abundance of *Firmicutes* in gastrointestinal trait. At the species level, the relative abundance of *Lactobacillus intestinalis* and *Lactobacillus sp. BL302* in KO + SDV group was higher than that of KO + sham group. Furthermore, network analysis showed that these two bacteria were correlated with depression-like phenotypes and reduced synaptic proteins, suggesting a role of these two bacteria in depression. In contrast, the relative abundance of *Turicibacter sp. LA62* in KO + SDV group was lower than that of KO + sham group. A network analysis showed that *Turicibacter sp. LA62* was also correlated with depression-like phenotypes and reduced synaptic proteins. Collectively, it seems that *Lactobacillus intestinalis*, *Lactobacillus sp. BL302*, and *Turicibacter sp. LA62* might be associated with depression-like phenotypes although further study is needed.

Using untargeted metabolomics analysis, we found that plasma levels of 1,5-anhydro-D-sorbitol (also known as 1,5-anhydro-D-glucitol), L-citrulline, and taurocholic acid in the KO + SDV group were higher than those of KO + sham group. A network analysis showed that 1,5-anhydro-D-sorbitol was negatively correlated with *Faecalibaculum rodentium*, suggesting that *Faecalibaculum rodentium* may be involved in the synthesis of 1,5-anhydro-D-sorbitol. A report showed that low plasma levels of 1,5-anhydro-D-sorbitol are closely associated with impaired peripheral nerve function and diabetic peripheral neuropathy in patients with type 2 diabetes (Xu et al., 2022), suggesting that lower plasma levels of 1,5-anhydro-D-sorbitol may be a risk factor for diabetic peripheral neuropathy. L-citrulline is a nitrogen end product produced from glutamine through urea cycle. Blood levels of L-citrulline and L-arginine in unmedicated patients with major depressive disorder (MDD) were significantly lower than healthy controls (Hess et al., 2017). MDD patients had a lower NOS (nitric oxide synthase) activity (L-citrulline/L-arginine ratio) than healthy controls at baseline (Loeb et al., 2020). NOS activity in MDD patients increased significantly after antidepressant treatment (Loeb et al., 2020), suggesting a state biomarker for depression. Furthermore, taurocholic acid (conjugation of cholic acid

with taurine) was positively correlated with several bacteria including *Lactobacillus intestinalis*, suggesting that these bacteria may play a role in the production of taurocholic acid, major bile acid. Interestingly, there was a significant difference in blood levels of taurocholic acid between MDD patients and healthy controls (Bai et al., 2021). Given anti-inflammatory role of taurocholic acid, it is possible that higher levels of taurocholic acid may play a role in antidepressant-like effects of SDV in *Chrna7* KO mice. Succinic anhydride was negatively correlated with *Bacteroides sp. TP-5* which were associated with depression-like phenotypes. Collectively, it is likely that microbes-derived metabolites may play a role in the antidepressant-like effects of SDV in *Chrna7* KO mice.

A network analysis showed that *Lactobacillus intestinalis*, *Lactobacillus reuteri*, *Turicibacter sp. LA62*, and *Bacteroides sp. TP-5* were correlated with depression-like behaviors. There are no reports showing the role of *Turicibacter sp. LA62*, and *Bacteroides sp. TP-5* in depression. We reported that oral ingestion of *Lactobacillus intestinalis* and *Lactobacillus reuteri* caused depression-like phenotypes in antibiotic-treated mice through gut–microbiota–brain axis via subdiaphragmatic vagus nerve (Wang et al., 2020a). Furthermore, we reported that oral ingestion of *Faecalibaculum rodentium* caused depression-like phenotypes in resilient *Ephx2* KO mice through gut–microbiota–brain axis via subdiaphragmatic vagus nerve (Wang et al., 2021). Furthermore, *Faecalibaculum rodentium* was positively correlated with FST data, and negatively correlated with SPT data. These data suggest that *Faecalibaculum rodentium* might play a role in depression-like phenotypes. Collectively, it is likely that these bacteria might play a role in the antidepressant-like effects of SDV in *Chrna7* KO mice although further study is needed.

This study has the one limitation. The current data of this study do not show a direct role of gut microbiota in depression-like phenotypes of *Chrna7* KO mice although a previous study suggests a role of gut microbiota in depression-like phenotypes of *Chrna7* KO mice (Pu Y, et al., 2021b). Further study to identify specific microbiomes which contribute to depression-like phenotypes of *Chrna7* KO mice is needed.

In conclusion, the current data show that SDV blocked depression-like behaviors and reduced

synaptic proteins in the mPFC of *Chrna7* KO mice. Therefore, gut–microbiota–brain axis via subdiaphragmatic vagus nerve plays a role in depression-like phenotypes in *Chrna7* KO mice.

Data and code availability

The 16S rRNA sequencing data has been uploaded and saved in the NCBI Sequence Read Archive and is available at the accession number PRJNA845101.

References

Andersson, U., Tracey, K.J., 2012. Reflex principles of immunological homeostasis. Annu. Rev. Immunol. 30, 313-335. doi: 10.1146/annurev-immunol-020711-075015.

Bai, S., Xie, J., Bai, H., Tian, T., Zou, T., Chen, J.J., 2021. Gut microbiota-derived inflammation-related serum metabolites as potential biomarkers for major depressive disorder. J. Inflamm. Res. 14, 3755–3766. doi: 10.2147/JIR.S324922.

Bartoli, F., Misiak, B., Callovini, T., Cavaleri, D., Cioni, R. M., Crocamo, C., Savitz, J. B., Carrà, G., 2021. The kynurenine pathway in bipolar disorder: a meta-analysis on the peripheral blood levels of tryptophan and related metabolites. Mol. Psychiatry 26(7), 3419–3429. doi: 10.1038/s41380-020-00913-1.

Bonaz, B., Bazin, T., Pellissier, S., 2018. The vagus nerve at the interface of the microbiota-gut-brain axis. Front. Neurosci. 12, 49. doi: 10.3389/fnins.2018.00049.

Brydges, C.R., Bhattacharyya, S., Dehkordi, S.M., Milaneschi, Y., Penninx, B., Jansen, R., Kristal, B.S., Han, X., Arnold, M., Kastenmüller, G., Bekhbat, M., Mayberg, H.S., Craighead, W.E., Rush, A.J., Fiehn, O., Dunlop, B.W., Kaddurah-Daouk, R., Mood Disorders Precision Medicine Consortium., 2022. Metabolomic and inflammatory signatures of symptom dimensions in major depression. Brain Behav. Immun. 102, 42-52. doi: 10.1016/j.bbi.2022.02.003.

Caso, J.R., MacDowell, K.S., González-Pinto, A., García, S., de Diego-Adeliño, J., Carceller-Sindreu, M., Sarramea, F., Caballero-Villarraso, J., Gracia-García, P., De la Cámara, C., Agüera, L., Gómez-Lus, M.L., Alba, C., Rodríguez, J.M., Leza, J.C., 2021. Gut microbiota, innate immune pathways, and inflammatory control mechanisms in patients with major depressive disorder. Transl. Psychiatry 11(1), 645. doi: 10.1038/s41398-021-01755-3.

Cawthon, C.R., de La Serre, C.B., 2018. Gut bacteria interaction with vagal afferents. Brain Res. 1693, 134–139. doi: 10.1016/j.brainres.2018.01.012.

Chang, L., Wei, Y., Hashimoto, K., 2022. Brain-gut-microbiota axis in depression: A historical overview and future directions. Brain Res Bull. 182, 44–56. doi: 10.1016/j.brainresbull.2022.02.004.

Cryan, J.F., O'Riordan, K.J., Cowan, C.S.M., Sandhu, K.V., Bastiaanssen, T.F.S., Boehme, M., Codagnone, M.G., Cussotto, S., Fulling, C., Golubeva, A.V., Guzzetta, K.E., Jaggar, M., Long-Smith, C.M., Lyte, J.M., Martin, J.A., Molinero-Perez, A., Moloney, G., Morelli, E., Morillas, E., O'Connor, R., Cruz-Pereira, J.S., Peterson, V.L., Rea, K., Ritz, N.L., Sherwin, E., Spichak, S., Teichman, E.M., van de Wouw, M., Ventura-Silva, A.P., Wallace-Fitzsimons, S.E., Hyland, N., Clarke, G., Dinan, T.G., 2019. The microbiota-gut-brain axis. Physiol. Rev. 99(4), 1877–2013. doi: 10.1152/physrev.00018.2018.

Dani, J.A., 2015. Neuronal nicotinic acetylcholine receptor structure and function and response to nicotine. Int. Rev. Neurobiol. 124, 3–19. doi: 10.1016/bs.irn.2015.07.001.

Dani, J.A., Bertrand, D., 2007. Nicotinic acetylcholine receptors and nicotinic cholinergic mechanisms of the central nervous system. Annu. Rev. Pharmacol. Toxicol. 47, 699-729. doi: 10.1146/annurev.pharmtox.47.120505.105214.

Forsythe, P., Bienenstock, J., Kunze, W.A., 2014. Vagal pathways for microbiome-brain-gut axis communication. Adv. Exp. Med. Biol. 817, 115–133. doi: 10.1007/978-1-4939-0897-4_5.

Haroon, E., Raison, C.L., Miller, A.H., 2012. Psychoneuroimmunology meets neuropsychopharmacology: translational implications of the impact of inflammation on behavior. Neuropsychopharmacology. 37(1), 137–162. doi: 10.1038/npp.2011.205.

Hashimoto, K., 2009. Emerging role of glutamate in the pathophysiology of major depressive disorder. Brain Res. Rev. 61(2), 105-123. doi: 10.1016/j.brainresrev.2009.05.005.

Hashimoto, K., 2015. Inflammatory biomarkers as differential predictors of antidepressant response. Int J Mol Sci. 16(4), 7796–7801. doi: 10.3390/ijms16047796.

Hashimoto, K., 2020. Molecular mechanisms of the rapid-acting and long-lasting antidepressant actions of (*R*)-ketamine. Biochem. Pharmacol. 177, 113935. doi: 10.1016/j.bcp.2020.113935.

Hashimoto, K., 2022. Gut–microbiota–brain by bile acids in depression. Psychiatry Clin. Neurosci., 76 (7) (2022), p. 281, 10.1111/pcn.13370.

Hess, S., Baker, G., Gyenes, G., Tsuyuki, R., Newman, S., Le Melledo, J.M., 2017. Decreased serum L-arginine and L-citrulline levels in major depression. Psychopharmacology (Berl) 234(21), 3241-3247. doi: 10.1007/s00213-017-4712-8.

Huang, N., Hua, D., Zhan, G., Li, S., Zhu, B., Jiang, R., Yang, L., Bi, J., Xu, H., Hashimoto, K., Luo, A., Yang, C., 2019. Role of *Actinobacteria* and *Coriobacteriia* in the antidepressant effects of ketamine in an inflammation model of depression. Pharmacol Biochem Behav. 176, 93–100. doi: 10.1016/j.pbb.2018.12.001.

Jiang, H., Ling, Z., Zhang, Y., Mao, H., Ma, Z., Yin, Y., Wang, W., Tang, W., Tan, Z., Shi, J., Li, L., Ruan, B., 2015. Altered fecal microbiota composition in patients with major depressive disorder. Brain Behav. Immun. 48, 186–194. doi: 10.1016/j.bbi.2015.03.016.

Kelly, J.R., Borre, Y., O' Brien, C., Patterson, E., El Aidy, S., Deane, J., Kennedy, P.J., Beers, S., Scott, K., Moloney, G., Hoban, A.E., Scott, L., Fitzgerald, P., Ross, P., Stanton, C., Clarke, G., Cryan, J. F., Dinan, T.G., 2016. Transferring the blues: Depression-associated gut microbiota induces neurobehavioural changes in the rat. J Psychiatr Res. 82, 109–118. doi: 10.1016/j.jpsychires.2016.07.019.

Lei, W., Duan, Z., 2021. Advances in the treatment of cholinergic anti-inflammatory pathways in gastrointestinal diseases by electrical stimulation of vagus nerve. Digestion 102(2), 128–138. doi: 10.1159/000504474.

Li, Z., Lai, J., Zhang, P., Ding, J., Jiang, J., Liu, C., Huang, H., Zhen, H., Xi, C., Sun, Y., Wu, L., Wang, L., Gao, X., Li, Y., Fu, Y., Jie, Z., Li, S., Zhang, D., Chen, Y., Zhu, Y., Lu, S., Lu, J., Wang, D., Zhou, H., Yuan, X., Li, X., Pang, L., Huang, M., Yang, H., Zhang, W., Brix, S., Kristiansen, K., Song, X., Nie, C., Hu, S., 2022. Multi-omics analyses of serum metabolome, gut microbiome and brain function reveal dysregulated microbiota-gut-brain axis in bipolar depression. Mol. Psychiatry 2022 April 20. doi: 10.1038/s41380-022-01569-9.

Liu, J.J., Wei, Y.B., Strawbridge, R., Bao, Y., Chang, S., Shi, L., Que, J., Gadad, B.S., Trivedi, M.H., Kelsoe, J.R., Lu, L., 2020. Peripheral cytokine levels and response to antidepressant treatment in depression: a systematic review and meta-analysis. Mol. Psychiatry 25(2), 339-350. doi: 10.1038/s41380-019-0474-5.

Loeb, E., El Asmar, K., Trabado, S., Gressier, F., Colle, R., Rigal, A., Martin, S., Verstuyft, C., Fève, B., Chanson, P., Becquemont, L., Corruble, E., 2020. Nitric Oxide Synthase activity in major depressive episodes before and after antidepressant treatment: Results of a large case-control treatment study. Psychol. Med. 2020 Jun 11:1-10. doi: 10.1017/S0033291720001749.

Lucido, M.J., Bekhbat, M., Goldsmith, D.R., Treadway, M.T., Haroon, E., Felger, J.C., Miller, A.H., 2021. Aiding and abetting anhedonia: Impact of inflammation on the brain and pharmacological implications. Pharmacol. Rev. 73(3), 1084–1117. doi: 10.1124/pharmrev.120.000043.

Mac Giollabhui, N., Ng, T.H., Ellman, L.M., Alloy, L.B., 2021. The longitudinal associations of inflammatory biomarkers and depression revisited: systematic review, meta-analysis, and meta-regression. Mol. Psychiatry 26(7), 3302-3314. doi: 10.1038/s41380-020-00867-4.

Martelli, D., McKinley, M.J., McAllen, R.M., 2014. The cholinergic anti-inflammatory pathway: a critical review. Auton. Neurosci. 182, 65–69. doi: 10.1016/j.autneu.2013.12.007.

McVey Neufeld, K.A., Bienenstock, J., Bharwani, A., Champagne-Jorgensen, K., Mao, Y., West, C., Liu, Y., Surette, M.G., Kunze, W., Forsythe, P., 2019. Oral selective serotonin reuptake inhibitors activate vagus nerve dependent gut-brain signalling. Sci. Rep. 9(1), 14290. doi: 10.1038/s41598-019-50807-8.

Miller, A.H., Raison, C.L., 2016. The role of inflammation in depression: from evolutionary imperative to modern treatment target. Nat. Rev. Immunol. 16(1), 22–34. doi: 10.1038/nri.2015.5.

Nikolova, V.L., Hall, M.R.B., Hall, L.J., Cleare, A.J., Stone, J.M., Young, A.H., 2021. Perturbations in gut microbiota composition in psychiatric disorders: a review and meta-analysis. JAMA Psychiatry 78(12), 1343-1354. doi: 10.1001/jamapsychiatry.2021.2573.

Olofsson, P.S., Rosas-Ballina, M., Levine, Y.A., Tracey, K.J., 2012. Rethinking inflammation: neural circuits in the regulation of immunity. Immunol. Rev. 248(1), 188–204. doi: 10.1111/j.1600-065X.2012.01138.x.

O'Mahony, C., van der Kleij, H., Bienenstock, J., Shanahan, F., O'Mahony, L., 2009. Loss of vagal anti-inflammatory effect: in vivo visualization and adoptive transfer. Am. J. Physiol. Regul. Integr. Comp. Physiol. 297(4), R1118–26. doi: 10.1152/ajpregu.90904.2008.

Park, A.J., Collins, J., Blennerhassett, P.A., Ghia, J.E., Verdu, E.F., Bercik, P., Collins, S.M., 2013. Altered colonic function and microbiota profile in a mouse model of chronic depression. Neurogastroenterol. Motil. 25(9), 733–e575. doi: 10.1111/nmo.12153.

Piovesana, R., Salazar Intriago, M.S., Dini, L., Tata, A.M., 2021. Cholinergic modulation of neuroinflammation: Focus on α7 nicotinic receptor. Int. J. Mol. Sci. 22(9), 4912. doi: 10.3390/ijms22094912.

Pu, J., Liu, Y., Zhang, H., Tian, L., Gui, S., Yu, Y., Chen, X., Chen, Y., Yang, L., Ran, Y., Zhong, X., Xu, S., Song, X., Liu, L., Zheng, P., Wang, H., Xie, P., 2021a. An integrated meta-analysis of peripheral blood metabolites and biological functions in major depressive disorder. Mol. Psychiatry 26(8), 4265–4276. doi: 10.1038/s41380-020-0645-4.

Pu, Y., Tan, Y., Qu, Y., Chang, L., Wang, S., Wei, Y., Wang, X., Hashimoto, K., 2021b. A role of the subdiaphragmatic vagus nerve in depression-like phenotypes in mice after fecal microbiota transplantation from *Chrna7* knock-out mice with depression-like phenotypes. Brain Behav. Immun. 94, 318–326. doi: 10.1016/j.bbi.2020.12.032.

Pu, Y., Zhang, Q., Tang, Z., Lu, C., Wu, L., Zhong, Y., Chen, Y., Hashimoto, K., Luo, Y., Liu Y., 2022. Fecal microbiota transplantation from patients with rheumatoid arthritis causes depression-like behaviors in mice through abnormal T cells activation. Transl. Psychiatry 12(1), 223. doi: 10.1038/s41398-022-01993-z.

Qu, Y., Yang, C., Ren, Q., Ma, M., Dong, C., Hashimoto, K., 2017. Comparison of (*R*)-ketamine and lanicemine on depression-like phenotype and abnormal composition of gut microbiota in a social defeat stress model. Sci Rep. 7(1), 15725. doi: 10.1038/s41598-017-16060-7.

Sanada, K., Nakajima, S., Kurokawa, S., Barceló-Soler, A., Ikuse, D., Hirata, A., Yoshizawa, A., Tomizawa, Y., Salas-Valero, M., Noda, Y., Mimura, M., Iwanami, A., Kishimoto, T., 2020. Gut

microbiota and major depressive disorder: A systematic review and meta-analysis. J. Affect. Disord. 266, 1-13. doi: 10.1016/j.jad.2020.01.102.

Schymanski, E.L., Jeon, J., Gulde, R., Fenner, K., Ruff, M., Singer, H.P., Hollender, J., 2014. Identifying small molecules via high resolution mass spectrometry: communicating confidence. Environ. Sci. Technol. 48(4), 2097–2098. doi: 10.1021/es5002105.

Segata, N., Izard, J., Waldron, L., Gevers, D., Miropolsky, L., Garrett, W.S., Huttenhower, C., 2011. Metagenomic biomarker discovery and explanation. Genome. Biol. 12(6), R60. doi: 10.1186/gb-2011-12-6-r60.

Shan, J., Hashimoto, K., 2022. Soluble epoxide hydrolase as a therapeutic target for neuropsychiatric disorders. Int. J. Mol. Sci. 23(9), 4951. doi: 10.3390/ijms23094951.

Toenders, Y.J., Laskaris, L., Davey, C.G., Berk, M., Milaneschi, Y., Lamers, F., Penninx, B.W.J.H., Schmaal, L., 2022. Inflammation and depression in young people: a systematic review and proposed inflammatory pathways. Mol. Psychiatry 27(1), 315-327. doi: 10.1038/s41380-021-01306-8.

Tran, S.M., Mohajeri, M.H., 2021. The role of gut bacterial metabolites in brain development, aging and disease. Nutrients 13(3), 732. doi: 10.3390/nu13030732.

Tsugawa, H., Cajka, T., Kind, T., Ma, Y., Higgins, B., Ikeda, K., Kanazawa, M., VanderGheynst, J., Fiehn, O., Arita, M., 2015. MS-DIAL: data-independent MS/MS deconvolution for comprehensive metabolome analysis. Nat. Methods 12(6), 523-526. doi: 10.1038/nmeth.3393.

Ulloa, L., 2005. The vagus nerve and the nicotinic anti-inflammatory pathway. Nat. Rev. Drug Discov. 4(8), 673–684. doi: 10.1038/nrd1797.

Wan, X., Eguchi, A., Fujita, Y., Ma, L., Wang, X., Yang, Y., Qu, Y., Chang, L., Zhang, J., Mori, C., Hashimoto, K., 2022a. Effects of (*R*)-ketamine on reduced bone mineral density in ovariectomized mice: a role of gut microbiota. Neuropharmacol. 213, 109139. doi: 10.1016/j.neuropharm.2022.109139.

Wan, X., Eguchi, A., Qu, Y., Yang, Y., Chang, L., Shan, J., Mori, C., Hashimoto, K., 2022b. Gut–microbiota–brain axis in the vulnerability to psychosis in adulthood after repeated cannabis exposure during adolescence. Eur. Arch. Psychiatry Clin. Neurosci. 272(7), 1297–1309. doi:10.1007/s00406-022-01437-1.

Wang, H., Yu, M., Ochani, M., Amella, C.A., Tanovic, M., Susarla, S., Li, J.H., Wang, H., Yang, H., Ulloa, L., Al-Abed, Y., Czura, C.J., Tracey, K.J., 2003. Nicotinic acetylcholine receptor α7 subunit is an essential regulator of inflammation. Nature. 421(6921), 384–388. doi: 10.1038/nature01339.

Wang, S., Ishima, T., Qu, Y., Shan, J., Chang, L., Wei, Y., Zhang, J., Pu, Y., Fujita, Y., Tan, Y., Wang, X., Ma, L., Wan, X., Hammock, B.D., Hashimoto, K., 2021. Ingestion of *Faecalibaculum rodentium* causes depression-like phenotypes in resilient *Ephx2* knock-out mice: A role of brain-gut-microbiota axis via the subdiaphragmatic vagus nerve. J Affect Disord. 292, 565–573. doi: 10.1016/j.jad.2021.06.006.

Wang, S., Ishima, T., Zhang, J., Qu, Y., Chang, L., Pu, Y., Fujita, Y., Tan, Y., Wang, X., Hashimoto, K., 2020a. Ingestion of *Lactobacillus intestinalis* and *Lactobacillus reuteri* causes depression- and anhedonia-like phenotypes in antibiotic-treated mice via the vagus nerve. J Neuroinflammation. 17(1), 241. doi: 10.1186/s12974-020-01916-z.

Wang, S., Qu, Y., Chang, L., Pu, Y., Zhang, K., Hashimoto, K., 2020b. Antibiotic-induced microbiome depletion is associated with resilience in mice after chronic social defeat stress. J Affect Disord. 260, 448–457. doi: 10.1016/j.jad.2019.09.064.

Wei, Y., Chang, L., Hashimoto, K., 2022a. Molecular mechanisms underlying the antidepressant actions of arketamine: beyond the NMDA receptor. Mol. Psychiatry 27(1), 559-573. doi: 10.1038/s41380-021-01121-1.

Wei, Y., Wang, T., Liao, L., Fan, X., Chang, L., Hashimoto, K., 2022b. Brain-spleen axis in health and diseases: A review and future perspective. Brain Res Bull. 182, 130–140. doi: 10.1016/j.brainresbull.2022.02.008.

WHO, 2021. Depression. https://www.who.int.news-room/fact-sheets/default/depression.

Wong, M.L., Inserra, A., Lewis, M.D., Mastronardi, C.A., Leong, L., Choo, J., Kentish, S., Xie, P., Morrison, M., Wesselingh, S.L., Rogers, G.B., Licinio, J., 2016. Inflammasome signaling affects anxiety- and depressive-like behavior and gut microbiome composition. Mol. Psychiatry 21(6), 797–805. doi: 10.1038/mp.2016.46.

Wu, Y.J., Wang, L., Ji, C.F., Gu, S.F., Yin, Q., Zuo, J., 2021. The role of α7 nAChR-mediated cholinergic anti-inflammatory pathway in immune cells. Inflammation. 44(3), 821–834. doi: 10.1007/s10753-020-01396-6.

Xu, F., Zhao, L.H., Wang, X.H., Wang, C.H., Yu, C., Zhang, X.L., Ning, L.Y., Huang, H.Y., Su, J.B., Wang, X.Q., 2022. Plasma 1,5-anhydro-D-glucitol is associated with peripheral nerve function and diabetic peripheral neuropathy in patients with type 2 diabetes and mild-to-moderate hyperglycemia. Diabetol. Metab. Syndr. 14(1), 24. doi: 10.1186/s13098-022-00795-z.

Yang, C., Fang, X., Zhan, G., Huang, N., Li, S., Bi, J., Jiang, R., Yang, L., Miao, L., Zhu, B., Luo, A., Hashimoto, K., 2019. Key role of gut microbiota in anhedonia-like phenotype in rodents with neuropathic pain. Transl. Psychiatry 9(1), 57. doi: 10.1038/s41398-019-0379-8.

Yang, C., Qu, Y., Fujita, Y., Ren, Q., Ma, M., Dong, C., Hashimoto, K., 2017. Possible role of the gut microbiota-brain axis in the antidepressant effects of (*R*)-ketamine in a social defeat stress model. Transl. Psychiatry 7(12), 1294. doi: 10.1038/s41398-017-0031-4.

Yang, C., Shirayama, Y., Zhang, J.C., Ren, Q., Yao, W., Ma, M., Dong, C., Hashimoto, K., 2015. R-ketamine: a rapid-onset and sustained antidepressant without psychotomimetic side effects. Transl. Psychiatry 5(9), e632. doi: 10.1038/tp.2015.136.

Yang, H., George, S.J., Thompson, D.A., Silverman, H.A., Tsaava, T., Tynan, A., Pavlov, V.A., Chang, E.H., Andersson, U., Brines, M., Chavan, S.S., Tracey, K.J., 2022a. Famotidine activates the vagus nerve inflammatory reflex to attenuate cytokine storm. Mol. Med. 28(1), 57. doi: 10.1186/s10020-022-00483-8.

Yang, Y., Ishima, T., Wan, X., Wei, Y., Chang, L., Zhang, J., Qu, Y., Hashimoto, K., 2022b. Microglial depletion and abnormalities in gut microbiota composition and short-chain fatty acids in mice after repeated administration of colony stimulating factor 1 receptor inhibitor PLX5622. Eur. Arch. Psychiatry Clin. Neurosci. 272(3), 483–495. doi: 10.1007/s00406-021-01325-0.

Zhang, J.C., Wu, J., Fujita, Y., Yao, W., Ren, Q., Yang, C., Li, S.X., Shirayama, Y., Hashimoto, K., 2014. Antidepressant effects of TrkB ligands on depression-like behavior and dendritic changes in mice after inflammation. Int J Neuropsychopharmacol. 18(4), pyu077. doi: 10.1093/ijnp/pyu077.

Zhang, J.C., Yao, W., Dong, C., Yang, C., Ren, Q., Ma, M., Hashimoto, K., 2017. Blockade of interleukin-6 receptor in the periphery promotes rapid and sustained antidepressant actions: a possible role of gut-microbiota-brain axis. Transl. Psychiatry 7(5), e1138. doi: 10.1038/tp.2017.112.

Zhang, J.C., Yao, W., Hashimoto, K., 2016a. Brain-derived neurotrophic factor (BDNF)-TrkB signaling in inflammation-related depression and potential therapeutic targets. Curr. Neuropharmacol. 14(7), 721–731. doi: 10.2174/1570159x14666160119094646.

Zhang, J.C., Yao, W., Ren, Q., Yang, C., Dong, C., Ma, M., Wu, J., Hashimoto, K., 2016b. Depression-like phenotype by deletion of α7 nicotinic acetylcholine receptor: Role of BDNF-TrkB in nucleus accumbens. Sci. Rep. 6, 36705. doi: 10.1038/srep36705.

Zhang, J., Ma, L., Chang, L., Pu, Y., Qu, Y., Hashimoto, K., 2020. A key role of the subdiaphragmatic vagus nerve in the depression-like phenotype and abnormal composition of gut microbiota in mice after lipopolysaccharide administration. Transl. Psychiatry10(1), 186. doi: 10.1038/s41398-020-00878-3.

Zhang, K., Fujita, Y., Chang, L., Qu, Y., Pu, Y., Wang, S., Shirayama, Y., Hashimoto, K., 2019. Abnormal composition of gut microbiota is associated with resilience versus susceptibility to inescapable electric stress. Transl. Psychiatry 9(1), 231. doi: 10.1038/s41398-019-0571-x.

Zheng, P., Zeng, B., Zhou, C., Liu, M., Fang, Z., Xu, X., Zeng, L., Chen, J., Fan, S., Du, X., Zhang, X., Yang, D., Yang, Y., Meng, H., Li, W., Melgiri, N.D., Licinio, J., Wei, H., Xie, P., 2016. Gut microbiome remodeling induces depressive-like behaviors through a pathway mediated by the host's metabolism. Mol. Psychiatry 21(6), 786–796. doi: 10.1038/mp.2016.44.

Progress in Neuro-Psychopharmacology and Biological Psychiatry
Volume 120, 10 January 2023, 110652
2022 年 09 月 30 日　公表済
DOI: 10.1016/j.pnpbp.2022.110652.